

## Article

# Exploring the Structural, Electronic, Magnetic, and Transport Properties of 2D Cr, Fe, and Zr Monoborides

Isabel M. Arias-Camacho  and Nevill Gonzalez Szwacki \* 

Faculty of Physics, University of Warsaw, Pasteura 5, PL-02093 Warsaw, Poland; isabel.arias@fuw.edu.pl

\* Correspondence: gonz@fuw.edu.pl; Tel.: +48-22-55-32-797

**Abstract:** Compared to other 2D materials, MBenes are at an early stage of investigation in terms of both experimental and theoretical approaches. However, their wide range of possible 2D structures leads to novel and challenging properties and consequent applications. From all the possible stoichiometries, we performed a theoretical study of orthorhombic and hexagonal  $M_2B_2$  MBenes within the framework of density functional theory. We found that both symmetries of  $Cr_2B_2$ ,  $Fe_2B_2$ , and  $Zr_2B_2$  show metallic behavior and could be grown under certain conditions as they were demonstrated to be dynamically stable. Moreover, the values of the magnetic moment observed, in specific ferromagnetic cases exceeding  $2.5 \mu_B/M_2B_2$ , make them suitable as robust 2D magnets. Our findings represent an important step in the understanding of MBenes and open several windows to future research in fields like energy conversion and storage, sensing, catalysis, biochemistry, and nanotechnology, among others.

**Keywords:** transition metal borides; MBenes; energy conversion and storage; 2D magnets



**Citation:** Arias-Camacho, I.M.; Gonzalez Szwacki, N. Exploring the Structural, Electronic, Magnetic, and Transport Properties of 2D Cr, Fe, and Zr Monoborides. *Materials* **2023**, *16*, 5104. <https://doi.org/10.3390/ma16145104>

Academic Editor: Dominique de Caro

Received: 31 May 2023

Revised: 12 July 2023

Accepted: 16 July 2023

Published: 20 July 2023



**Copyright:** © 2023 by the authors. Licensee MDPI, Basel, Switzerland. This article is an open access article distributed under the terms and conditions of the Creative Commons Attribution (CC BY) license (<https://creativecommons.org/licenses/by/4.0/>).

## 1. Introduction

Transition metal borides (MBs) can be regarded as new efficient earth-abundant materials for energy storage/conversion systems, including metal-ion batteries, metal-air batteries, capacitors, oxygen evolution reactions (OERs), and other electrochemical fields [1]. Single-crystalline ternary transition metal borides (MAB phases, where M are transition metals, A are *p*-block elements, and B is boron) were first reported in 2015 by Ade and Hillebrecht and recently gained attention as promising layered materials [2]. Their two-dimensional counterparts (MBenes) can be obtained from the chemical exfoliation of the MAB phases. It is noted that MBenes possess different stoichiometries and variable modes of 2D layer sandwiching compared to the corresponding MXenes [3].

The MAB phases with M and B with one-to-one stoichiometry are orthorhombic and hexagonal crystals with the chemical formulae of MAB and  $M_2AB_2$  [3]. Experimentally, orthorhombic MAIB (M = Mo and W),  $M_2AlB_2$  (M = Cr, Mn, and Fe), and hexagonal  $Ti_2InB_2$  [4] have already been synthesized. The MAB phases are promising candidates for obtaining new 2D MBenes. A 2D MoB was reported to have been obtained by the partial etching of  $Mo_2AlB_2$  phases through the deintercalation of Al layers from the ordered stacking faults region [5,6]. Selectively HCl-etching Al layers from  $Cr_2AlB_2$  yielded bulk-layered CrB nanosheets [7,8]. Removal of the indium layer through the high-temperature dealloying of  $Ti_2InB_2$  yielded a bulk-layered TiB structure [4]. To date, however, the synthesis of individual single-layer MBenes has not been realized.

The present work concerns computational studies of the structural, energetic, electronic, and transport properties of selected MBene compounds with M = Cr, Fe, and Zr. Some of the investigated 2D structures have been proven to be stable in previous studies [9]. The studied MBenes present either an orthorhombic structure (ortho-MBenes) with *Pmma* (no. 51) space group symmetry or a hexagonal structure (hex-MBenes) with *P6/mmm* (no. 191) space group symmetry. In the *Pmma* structures, each atom is surrounded by

six neighbors, and the buckled bilayers are sandwiched between transition metal (TM) layers. On the other hand, in the  $P6/mmm$  structures, the honeycomb-type boron layer is sandwiched between two TM layers on both sides, and every TM atom is located above or below the centroid of the honeycomb structure.

The bulk counterparts of our metal monoboride nanosheets are the ferromagnetic  $\alpha$  and  $\beta$  modifications of FeB and the nonmagnetic CrB and ZrB compounds, all widely studied, both experimentally and theoretically [10–12]. The structure of  $\alpha$ -FeB is debatable [12], whereas  $\beta$ -FeB and CrB are orthorhombic crystals with  $Pnma$  (no. 62) and  $Cmcm$  (no. 63) space group symmetries, respectively. The ZrB solid is rock-salt-structured and crystallizes in a cubic  $Fm\bar{3}m$  (no. 225) space group symmetry. The  $\beta$ -FeB and CrB solids exhibit very interesting structures since both enclose boron double-chain (BDC) stripes which are very common motifs of all-boron nanostructures [13,14].

The purpose of this work is to understand the origin of the physical properties of MBene (M = Cr, Fe, and Zr) compounds, as well as to identify features that may affect the transport properties of these compounds.

## 2. Computational Approach

First-principles spin-polarized calculations were performed within the framework of density functional theory (DFT) within the generalized gradient corrected approximation of Perdew–Burke–Ernzerhof (PBE) [15] for the exchange–correlation functional, using projector plane-wave (PAW) pseudopotentials [16] as implemented in the Quantum ESPRESSO (QE) suite of codes [17]. Every unit cell consists of two atoms of boron and two atoms of the TM. To avoid interactions between adjacent MBenes, we considered an empty space of thickness 15 Å along the normal direction. Optimized geometries were reached allowing the unit cell shape, volume, and the ions to relax until the residual forces on the atoms were less than 0.3 meV/Å and the total energy ( $E_{tot}$ ) convergence was set to  $10^{-5}$  Ry. We expanded the electronic wave functions and charge density in plane-wave basis sets with an energy cutoff of 70 and 700 Ry, respectively, while the  $\Gamma$ -centered  $k$ -point grid in the Brillouin zone, in the Monkhorst–Pack scheme, was set to  $12 \times 12 \times 1$  for the geometry optimization and  $24 \times 24 \times 1$  for the DOS calculations, with Gaussian smearing of 0.02 Ry; these values ensure the accuracy of  $E_{tot}$ . All the structures were considered to be initially spin-polarized and, in order to determine the magnetic ground states of each, we calculated two magnetic configurations—one ferromagnetic (FM) and one antiferromagnetic (AFM)—to reach the most energetically favorable.

For the structural characterization of the studied systems, an important descriptor we use is the cohesive energy per atom ( $E_{coh}$ ); that is, the difference in energy between  $E_{tot}$  of the compound and the sum of the total energies of the isolated atoms,

$$E_{coh} = (E[M_2B_2] - n_B E[B] - n_M E[M]) / (n_B + n_M), \quad (1)$$

which means the released energy when a compound dissociates into isolated free atoms, where M represents the TM atom,  $E[M_2B_2]$  is the  $E_{tot}$  of the MBene,  $E[B]$  and  $E[M]$  are the total energies of the isolated atoms (B and TM atoms), and  $n_B$  and  $n_M$  are the numbers of boron and TM atoms per unit cell, respectively, directly obtained from the spin-polarized calculations. The phonon-dispersion curves were obtained by means of density functional perturbation theory (DFPT), calculating the dynamical matrices in the linear response approach on a  $q$ -point grid of  $4 \times 4 \times 1$ . The transport integrals were computed using Boltzmann transport theory and a constant scattering rate model [18]. The charge transfer was obtained by Bader analysis [19] and all the visualizations were performed using the Visualization for Electronic and Structural Analysis (VESTA) software [20].

## 3. Results and Discussion

### 3.1. Structure and Stability

Since boron is electron deficient, it is expected that a mixture with TM atoms will lead to stable structures. As mentioned above, among all the possible MBenes, we focused on

those which possess either orthorhombic or hexagonal  $M_2B_2$  structures, which are shown in Figure 1. After a full structural optimization, we found that the unit cells of ortho-MBenes became almost rectangular with  $a > b$  when the TM was Fe or Cr ( $a/b$  is 1.005 and 1.013 for chromium and iron, respectively), whereas  $a < b$  for ortho- $Zr_2B_2$  ( $a/b = 0.94$ ). All the cell parameters are described in Table 1 and compared with other literature reports.

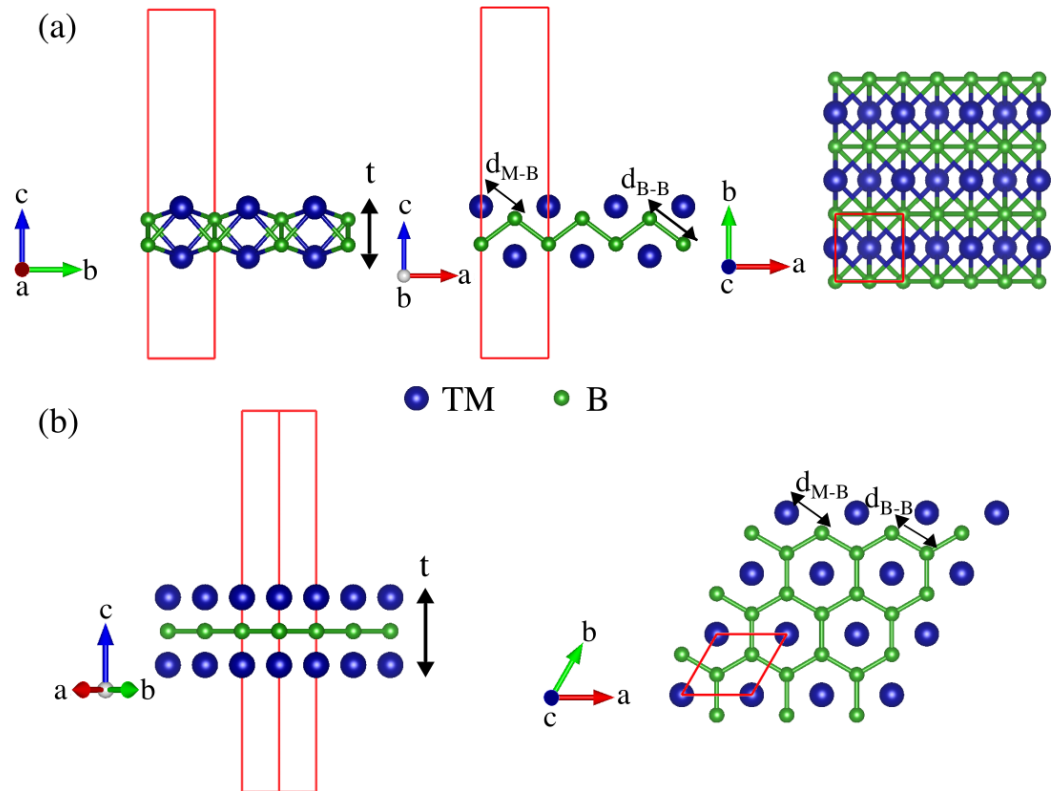


**Figure 1.** Side (left) and top (right) views of the (a) ortho-MBene and (b) hex-MBene structures of  $M_2B_2$  corresponding to  $Pnma$  and  $P6/mmm$  symmetries, respectively. The unit cells used in the calculations are shown in red.

The  $E_{coh}$  and phonon dispersion curves are good indicators of the bond strength and dynamical stability of the materials. The dynamical matrix gives us the frequency  $\omega(\mathbf{q})$  whose square is negative when there exist instabilities for a particular phonon mode with  $\mathbf{q}$  (imaginary frequencies), which means that this mode does not generate the restoring force needed by the lattice vibrations and could take the structure away from the original configuration. The results of our calculations are summarized in Table 2 and in Figure 2.

**Table 1.** Lattice parameters ( $a$  and  $b$ ), boron–boron distance ( $d_{B-B}$ ), TM–boron distance ( $d_{M-B}$ ), and thickness of the 2D structure ( $t$ ) for  $Cr_2B_2$ ,  $Fe_2B_2$ , and  $Zr_2B_2$ . The  $d_{B-B}$ ,  $d_{M-B}$ , and  $t$  parameters are defined in Figure 1. All the values are in Angstroms ( $\text{\AA}$ ) and, for comparison purposes, the data in brackets are taken from the literature.

	$Cr_2B_2$		$Fe_2B_2$		$Zr_2B_2$	
	$Pnma$	$P6/mmm$	$Pnma$	$P6/mmm$	$Pnma$	$P6/mmm$
$a$	2.885	2.919	2.823	2.913	3.084	3.159
	(2.860 <sup>4</sup> )	(2.921 <sup>1</sup> )	(2.800 <sup>4</sup> )		(3.07 <sup>7</sup> )	(3.144 <sup>1</sup> )
	(2.930 <sup>5</sup> )	(2.926 <sup>2</sup> )	(2.770 <sup>5</sup> )			(3.160 <sup>2</sup> )
						(3.134 <sup>3</sup> )

**Table 1.** Cont.

	<b>Cr<sub>2</sub>B<sub>2</sub></b>		<b>Fe<sub>2</sub>B<sub>2</sub></b>		<b>Zr<sub>2</sub>B<sub>2</sub></b>	
<i>b</i>	2.870	2.919	2.787	2.913	3.281	3.159
	(2.850 <sup>4</sup> )	(2.921 <sup>1</sup> )	(2.680 <sup>4</sup> )		(3.27 <sup>7</sup> )	(3.144 <sup>1</sup> )
	(2.870 <sup>5</sup> )	(2.926 <sup>2</sup> )	(2.820 <sup>5</sup> )			(3.160 <sup>2</sup> ) (3.134 <sup>3</sup> )
<i>d<sub>B-B</sub></i>	1.810	1.685	1.813	1.682	1.721	1.824
		(1.689 <sup>2</sup> )			(1.71 <sup>7</sup> )	(1.825 <sup>2</sup> ) (1.891 <sup>3</sup> )
<i>d<sub>M-B</sub></i>	2.10	2.15	2.04	2.15	2.46	2.49
	(2.11 <sup>4</sup> )		(2.05 <sup>4</sup> )		(2.43 <sup>7</sup> )	(2.49 <sup>3</sup> )
<i>t</i>	2.122	2.662	2.134	2.680	2.817	3.382
		(2.651 <sup>1</sup> )	(2.13 <sup>6</sup> )		(2.84 <sup>7</sup> )	(3.391 <sup>1</sup> )
		(2.639 <sup>2</sup> )				(3.380 <sup>2</sup> ) (3.385 <sup>3</sup> )

<sup>1</sup> Ref. [21]. <sup>2</sup> Ref. [22]. <sup>3</sup> Ref. [23]. <sup>4</sup> Ref. [24]. <sup>5</sup> Ref. [25]. <sup>6</sup> Ref. [26]. <sup>7</sup> Ref. [27].

**Table 2.** Cohesive energy ( $E_{coh}$ ), highest frequency at the  $\Gamma$  point ( $\nu$ ), and charge transfer from TM to B ( $\Delta q$ ) for Cr<sub>2</sub>B<sub>2</sub>, Fe<sub>2</sub>B<sub>2</sub>, and Zr<sub>2</sub>B<sub>2</sub>. The values in bold are to highlight the structure with higher  $E_{coh}$ .

	<b>Cr<sub>2</sub>B<sub>2</sub></b>		<b>Fe<sub>2</sub>B<sub>2</sub></b>		<b>Zr<sub>2</sub>B<sub>2</sub></b>	
	<i>Pmma</i>	<i>P6/mmm</i>	<i>Pmma</i>	<i>P6/mmm</i>	<i>Pmma</i>	<i>P6/mmm</i>
$E_{coh}$ (eV)	<b>6.222</b>	6.201	<b>6.901</b>	6.830	8.050	<b>8.087</b>
$\nu$ (cm <sup>-1</sup> )	762.45	1003.50	772.74	976.01	928.02	744.12
$\Delta q$ (e)	-0.76	-0.61	-0.37	-0.40	-1.17	-0.86

All our MBenes exhibit large  $E_{coh}$  values ranging from 6.222 to 8.087 eV, as shown in Table 2, which means they present strong internal binding and good stability. Moreover, our results are in good agreement with previous works. For instance, Zhang et al. [28] obtained a value of 6.30 eV for ortho-Cr<sub>2</sub>B<sub>2</sub>. For the sake of comparison, we also computed the diamond structure of carbon using the same optimization parameters, resulting in a  $E_{coh}$  of 7.757 eV, which is a comparable value to that of other theoretical and experimental reports [29]. Interestingly, other studies have noted a dependence of the structure stability with the atomic mass of the TM [22], a fact that is also reproduced in our results, hex-Zr<sub>2</sub>B<sub>2</sub> being the MBene with the highest  $E_{coh}$  (8.087 eV). From a structural point of view, Cr<sub>2</sub>B<sub>2</sub> and Fe<sub>2</sub>B<sub>2</sub> prefer to adopt orthorhombic structures, whereas Zr<sub>2</sub>B<sub>2</sub> accommodates better to the hexagonal one. However, the orthorhombic and hexagonal phases are close in energy (within some tens of meV), and, according to recent reports [9,30], ortho-MBenes might transform into hex-MBenes at high temperatures.

On the one hand, calculations of the phonon frequencies reveal that some small imaginary frequencies appear in the surroundings of the  $\Gamma$  point for orthorhombic Cr<sub>2</sub>B<sub>2</sub> and Zr<sub>2</sub>B<sub>2</sub> as shown on the left panel of Figure 2. On the other hand, none of the hexagonal structures have imaginary frequencies as shown on the right panel of Figure 2. Similar dynamical instabilities as for ortho-MBenes have been reported for freestanding 2D structures in previous works [25,31]. These studies have concluded that the out-of-plane acoustic mode, ZA, is responsible for such instabilities, which are against the long-wavelength transversal waves that could be fixed by defects like grain boundaries or ripples [32].

The highest values of the frequencies at the  $\Gamma$ -point are collected in Table 2. All the frequencies are higher than 740 cm<sup>-1</sup>. Starting with the orthorhombic structures, the highest optical frequency at  $\Gamma$ -point increases with the atomic number of the TM atom; that is, Cr, Fe, and Zr, in that order. These results are very close to those found in the literature [24]. Since the optical frequency is an indicator of the bond strength, Zr<sub>2</sub>B<sub>2</sub> is more stable than Cr<sub>2</sub>B<sub>2</sub> and Fe<sub>2</sub>B<sub>2</sub>. The trend is, however, the opposite for hex-mBenes, meaning that the

highest frequency at the  $\Gamma$ -point corresponds to the TM atom which has the smallest atomic number, in this case Cr, and decreases for Fe and Zr. We can conclude that the studied MBenes are stable and could be grown experimentally under certain conditions.

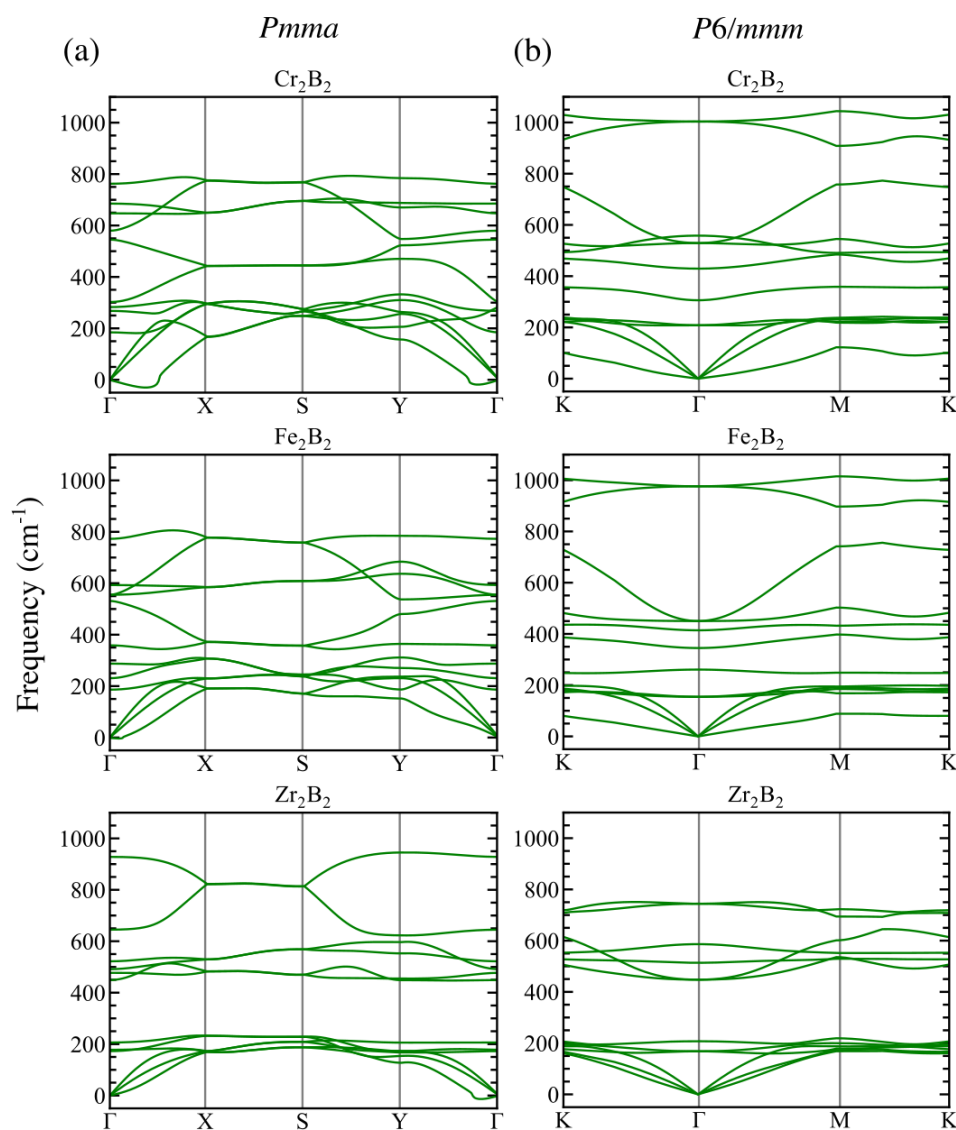


**Figure 2.** Phonon dispersion relations for the (a) *Pmma* and (b) *P6/mmm* structures of  $\text{Cr}_2\text{B}_2$ ,  $\text{Fe}_2\text{B}_2$ , and  $\text{Zr}_2\text{B}_2$ .

### 3.2. Electronic Properties

To understand the electronic behavior of the MBenes involved in our study, we calculated the spin-polarized band structure, the density of states (DOS), and the projected density of states (PDOS) for the studied systems. The results of these calculations are shown in Figures 3 and 4 for ortho-MBenes and hex-MBenes, respectively. Looking at the band structure and DOS, we may conclude that there are no band gaps between the valence band (VB) and the conduction band (CB) for any of the studied structures, which means that all the systems are metallic with partially occupied bands crossing the Fermi level (for the majority and the minority spin channels). This metallic character of the pristine MBenes has also been reported in other works [33]. In all cases, the  $p$  orbitals of boron are deep in energy (ranging from  $-8$  to  $-2$  eV approximately) and, in the orthorhombic structures, partially hybridize with the  $d$  orbitals of the TM. Near the Fermi level, the PDOS for both symmetries of  $\text{Cr}_2\text{B}_2$  and  $\text{Fe}_2\text{B}_2$  is dominated by the  $d$  orbitals of Cr and Fe, respectively (see the right panels of (a) and (b) in Figures 3 and 4). Whereas, hybridization between

the  $p$  and  $d$  orbitals of Zr occurs at the Fermi level of  $Zr_2B_2$  (see the right panels of (c) in Figures 3 and 4). The contribution of the majority states at the Fermi level of ortho- $Fe_2B_2$  is very small, whereas an equal contribution of the minority and majority states is observed in hex- $Fe_2B_2$  and also in both symmetries of  $Zr_2B_2$ . Finally, the contribution of the majority states is larger than that of the minority states at the Fermi level for  $Cr_2B_2$ .

According to our Bader analysis, the charge transfer,  $\Delta q$ , always occurs from the TMs to the boron atoms. This is shown in Table 2 where we present the values of  $\Delta q$  for all the studied cases. The obtained values are in agreement with other reports (e.g.,  $\Delta q = -0.34e$  for ortho- $Fe_2B_2$ , as reported in ref. [26]). In general, considering both the  $Pmma$  and  $P6/mmm$  structures, the largest charge transfer occurs between Zr and B, whereas Fe is the TM for which the charge transfer to B is the smallest one.

The conductivity results are shown in Figure 5. They reveal anisotropy of the conductivity tensor for the ortho-MBenes, especially for the case of ortho- $Zr_2B_2$  for which the direction perpendicular to the BDC is clearly the preferred one, whereas for ortho- $Fe_2B_2$ , the conductivity is higher along the BDC. On the other hand, the hex-MBenes are isotropic with respect to conductivity. It is also worth highlighting that the orthorhombic  $Fe_2B_2$  and  $Zr_2B_2$  present the highest conductivity values among all the studied cases.

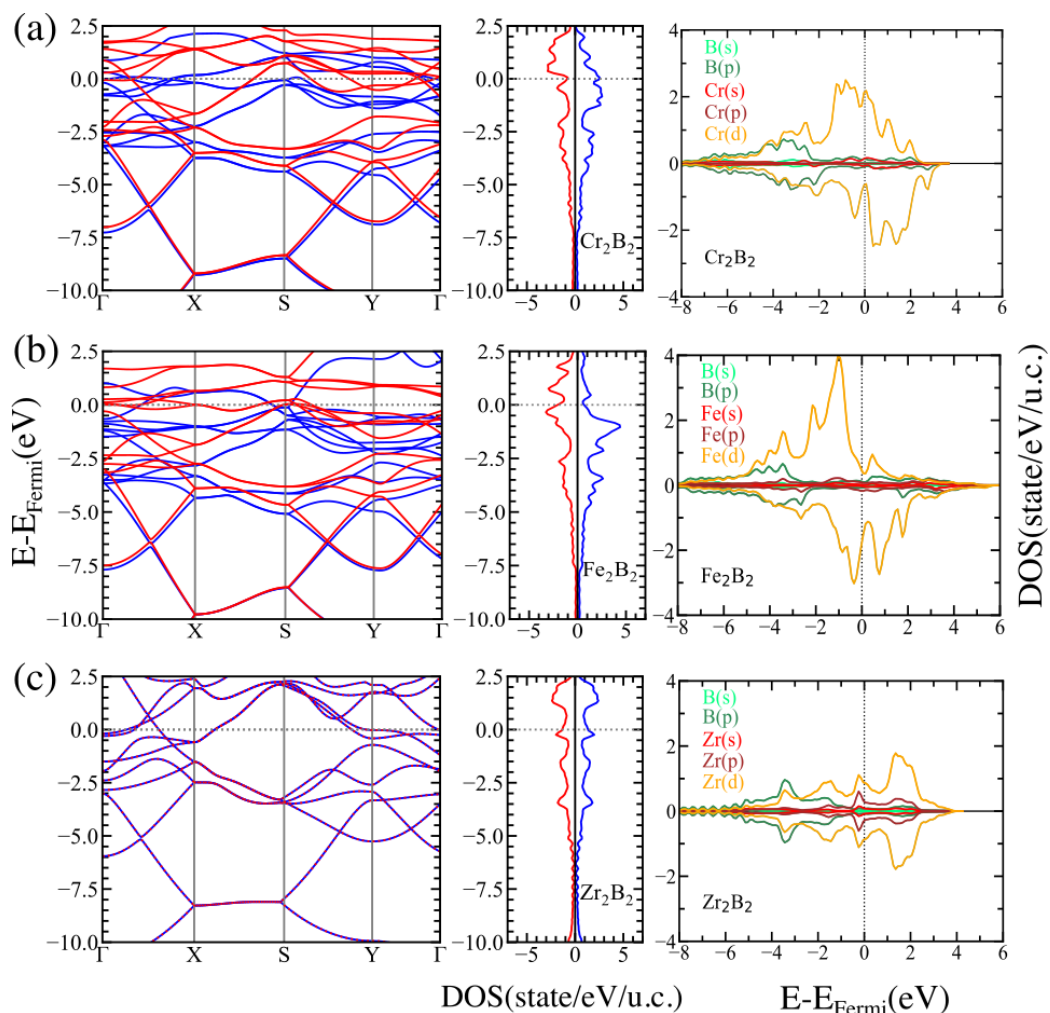


**Figure 3.** Electronic band structure (left) and DOS (center) for the majority (blue) and minority (red) spin states, and orbital-resolved PDOS (right) for the  $Pmma$  structures of (a)  $Cr_2B_2$ , (b)  $Fe_2B_2$ , and (c)  $Zr_2B_2$ .

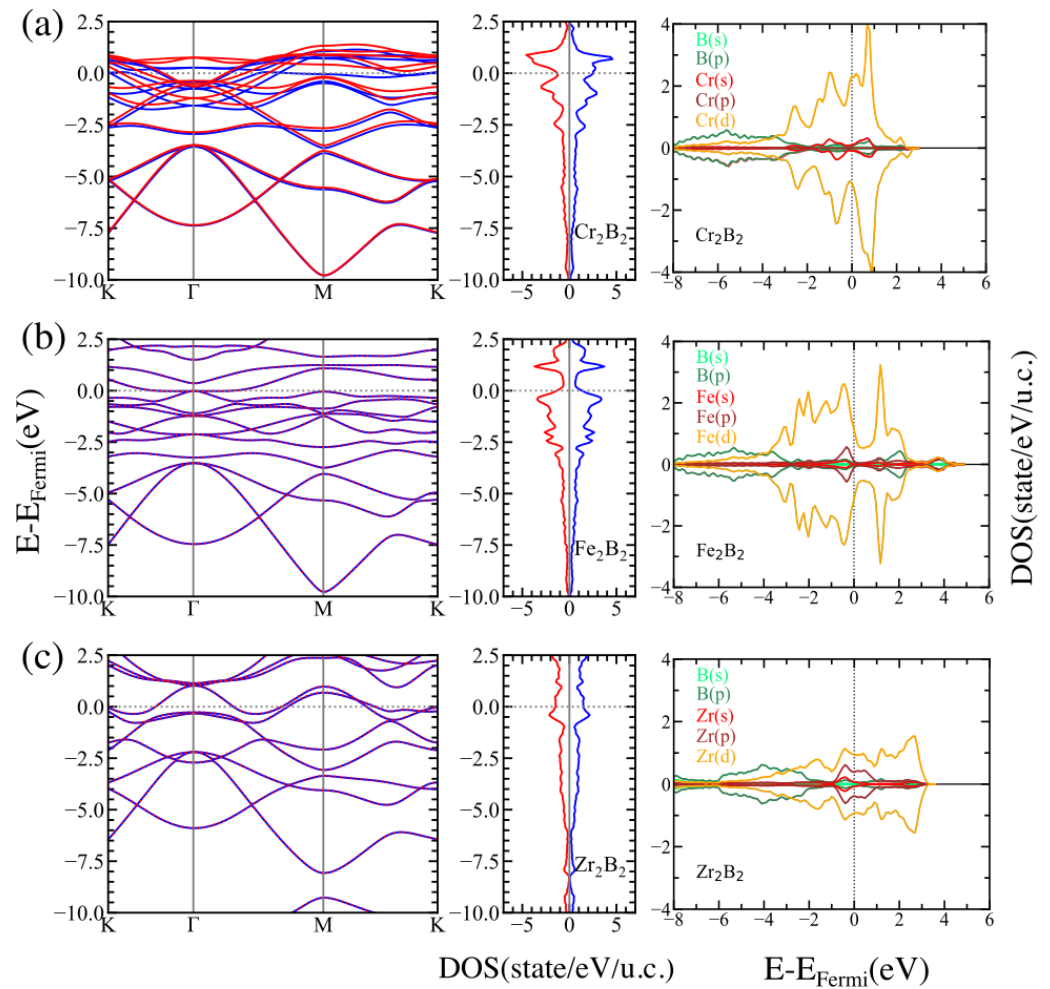


**Figure 4.** Electronic band structure and DOS for the majority (blue) and minority (red) spins, and orbital-resolved projected density of states (PDOS) for the  $P6/mmm$  structures of (a)  $\text{Cr}_2\text{B}_2$ , (b)  $\text{Fe}_2\text{B}_2$ , and (c)  $\text{Zr}_2\text{B}_2$ .

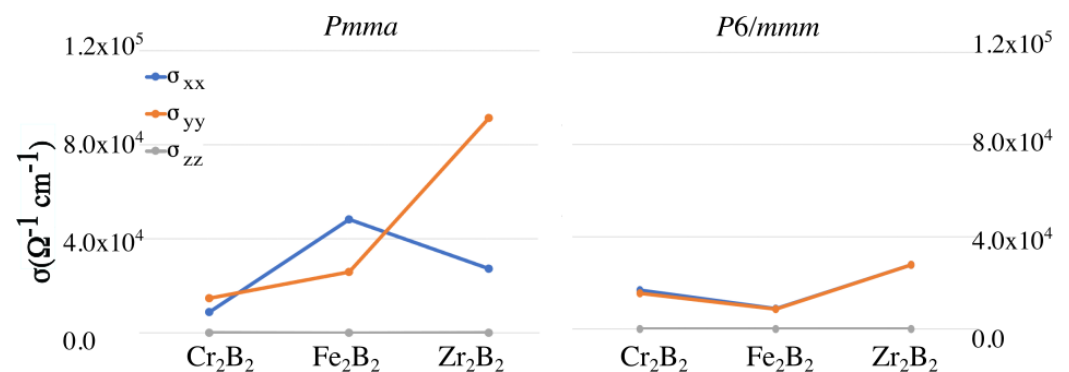


**Figure 5.** Components of the conductivity tensor for the  $Pmma$  (left) and  $P6/mmm$  (right) structures of  $\text{Cr}_2\text{B}_2$ ,  $\text{Fe}_2\text{B}_2$ , and  $\text{Zr}_2\text{B}_2$ .

### 3.3. Magnetic Properties

The origin of magnetism in these types of materials arises from the  $d$  orbitals of the TM atoms. Both FM and AFM configurations have been suggested to determine the ground state. The results of our calculations are summarized in Table 3. Among all the considered structures, only the hex- $\text{Fe}_2\text{B}_2$  resulted in an AFM ground state since the  $E_{tot}$  value of the FM state is 46.84 meV higher in energy. On the other hand, ortho- $\text{Fe}_2\text{B}_2$  exhibited an FM ground state in accordance with previous reports [34]. However, a more detailed analysis, that

also included the next nearest neighbors and was performed using DFT combined with the Monte Carlo method, revealed that ortho-Fe<sub>2</sub>B<sub>2</sub> actually has a stable columnar AFM ground state [26]. In the particular case of Cr<sub>2</sub>B<sub>2</sub>, both structures result in an FM arrangement of the magnetic moments. In general, the total energy difference,  $\Delta E_{\text{FM-AFM}}$ , between the FM and AFM configurations is always higher in absolute value for the orthorhombic structures (−104.38 and −108.12 eV for Cr<sub>2</sub>B<sub>2</sub> and Fe<sub>2</sub>B<sub>2</sub>, respectively,) than for the hexagonal ones (−0.29 and 46.84 eV for Cr<sub>2</sub>B<sub>2</sub> and Fe<sub>2</sub>B<sub>2</sub>, respectively) indicating that, in the latter case, the magnetic ordering may not be preserved at room temperature. Both orthorhombic Cr<sub>2</sub>B<sub>2</sub> and Fe<sub>2</sub>B<sub>2</sub> structures show an FM ground state with a magnetic moment over 2.5  $\mu_{\text{B}}$  per unit cell, a suitable behavior for robust 2D magnets. Interestingly, the boron atoms are also slightly polarized for those cases for which the TM–boron distances ( $d_{\text{M-B}}$ ) are the shortest (see Table 1). Finally, Zr<sub>2</sub>B<sub>2</sub> MBenes exhibit non-magnetic behavior.

The energy difference  $\Delta E_{\text{FM-AFM}} = E_{\text{FM}} - E_{\text{AFM}}$  can be used to evaluate the exchange interaction,  $J_{\text{NN}}$ , between TM atoms at the nearest neighbor (NN) positions. The exchange energy for a system of interacting atomic moments,  $\mathbf{S}_i$ , can be described by the Heisenberg model:

$$E_{\text{tot}} = E_0 - \frac{1}{2} \sum_{i \neq j} J_{ij} \mathbf{S}_i \cdot \mathbf{S}_j, \quad (2)$$

where  $E_0$  is the total energy excluding spin–spin interactions and in our case  $S_i = S_j = S$ . For ferromagnetically or antiferromagnetically coupled TM ions at NN positions  $-2J_{\text{NN}}S^2 = \Delta E_{\text{FM-AFM}}$ . The critical temperature (Curie or Néel temperature),  $T_c$ , in the mean field approximation (MFA) can be estimated from

$$T_c \simeq \frac{2}{3} k_{\text{B}} \cdot (J_{\text{NN}} S^2) = \frac{1}{3} k_{\text{B}} \cdot |\Delta E_{\text{FM-AFM}}|. \quad (3)$$

The  $T_c$  values are collected in Table 3. As can be seen from the table, we obtain a considerably large value of  $T_c = 418$  K for ortho-Fe<sub>2</sub>B<sub>2</sub>. However, as mentioned above, a more accurate investigation [26] predicts an AFM ground state with  $T_c = 115$  K. Interestingly, our calculations predict an AFM ground state for hex-Fe<sub>2</sub>B<sub>2</sub> with  $T_c = 181$  K.

**Table 3.** Total magnetic moment ( $\mu_{\text{tot}}$ ), magnetic moment of the TM atoms ( $\mu_{\text{TM}}$ ), magnetic moment induced on the boron atoms ( $\mu_{\text{B}}$ ), magnetic ground state (MGS), the total energy difference between the FM and the AFM configurations ( $\Delta E_{\text{FM-AFM}}$ ), and the critical temperature ( $T_c$ ) estimated using Equation (3) for Cr<sub>2</sub>B<sub>2</sub>, Fe<sub>2</sub>B<sub>2</sub>, and Zr<sub>2</sub>B<sub>2</sub>.

	Cr <sub>2</sub> B <sub>2</sub>		Fe <sub>2</sub> B <sub>2</sub>		Zr <sub>2</sub> B <sub>2</sub>	
	<i>Pnma</i>	<i>P6/mmm</i>	<i>Pnma</i>	<i>P6/mmm</i>	<i>Pnma</i>	<i>P6/mmm</i>
$\mu_{\text{tot}}$ ( $\mu_{\text{B}}$ /unit cell)	2.56	0.63	2.69	0.00	0.00	0.00
$\mu_{\text{TM}}$ ( $\mu_{\text{B}}$ /ion)	1.03	0.31	1.26	2.06/−2.06	0.00	0.00
$\mu_{\text{B}}$ ( $\mu_{\text{B}}$ /ion)	−0.05	−0.01	−0.05	0.00	0.00	0.00
MGS	FM	FM	FM	AFM	Non-magnetic	Non-magnetic
$\Delta E_{\text{FM-AFM}}$ (meV/unit cell)	−104.38	−0.29	−108.12	46.84	-	-
$T_c$ (K)	403	1	418	181	-	-

#### 4. Summary and Conclusions

In summary, we carried out a comparison between the structural, electronic, magnetic, and transport properties for orthorhombic and hexagonal phases of a selected group of MBenes, Cr<sub>2</sub>B<sub>2</sub>, Fe<sub>2</sub>B<sub>2</sub> and Zr<sub>2</sub>B<sub>2</sub>, that are usually considered separately in the literature. Although there are several theoretical reports that have predicted the stability of the studied MBenes, to our knowledge, hex-Fe<sub>2</sub>B<sub>2</sub> is shown for the first time in this work to be

dynamically stable. Experimentally the most studied MBenes are those composed of early TMs, whereas those composed of late TMs (like iron) remain to be synthesized.

We observe that, from an energetic point of view, the larger the atomic weight is, the higher the  $E_{coh}$  is, which means that  $Zr_2B_2$  possesses the strongest bonds. However, despite the small difference between the  $E_{coh}$  values of the orthorhombic and hexagonal structures of each MBene, both phases can exist theoretically. This assumption is reinforced by the calculation of the corresponding phonon dispersion plots that predict stable behavior of all the MBenes. Furthermore, the metallic character of our pristine MBenes makes them efficient materials for charge transport, and therefore are competitive 2D materials for electronic, sensing, or electrocatalytic purposes. We predicted that, for both symmetries of  $Cr_2B_2$ , the contribution of the majority spin states would be larger than that of the minority spin states at the Fermi level, leading to an FM ground state and opening the possibility of their use in information magnetic storage.

This understanding of the properties of the studied materials, together with the acknowledgment that, within the same framework, both orthorhombic and hexagonal phases are feasible and different in their properties, creates the possibility of going further in our research to consider them as potential candidates for sensing and catalytic processes. Although there exists some parallelism with MXenes, MBenes are emerging 2D materials that are expected to have great development potential in the future, due to their diverse stoichiometries and, as a consequence, structural differences and new challenging physical, chemical, and biological properties. The biggest difference for MBenes is that some of them can potentially exist in both orthorhombic and hexagonal phases.

**Author Contributions:** Conceptualization, I.M.A.-C. and N.G.S.; methodology, I.M.A.-C.; validation, I.M.A.-C.; investigation, I.M.A.-C. and N.G.S.; writing and original draft preparation, I.M.A.-C.; writing, review, and editing, N.G.S.; visualization, I.M.A.-C.; supervision, N.G.S. All authors have read and agreed to the published version of the manuscript.

**Funding:** This research received no external funding.

**Acknowledgments:** The use of supercomputers at the Interdisciplinary Centre for Mathematical and Computational Modelling (ICM) at the University of Warsaw is gratefully acknowledged.

**Conflicts of Interest:** The authors declare no conflict of interest.

## References

1. Akopov, G.; Yeung, M.T.; Kaner, R.B. Rediscovering the Crystal Chemistry of Borides. *Adv. Mater.* **2017**, *29*, 1604506. [[CrossRef](#)] [[PubMed](#)]
2. Ade, M.; Hillebrecht, H. Ternary Borides  $Cr_2AlB_2$ ,  $Cr_3AlB_4$ , and  $Cr_4AlB_6$ : The First Members of the Series  $(CrB_2)_nCrAl$  with  $n = 1, 2, 3$  and a Unifying Concept for Ternary Borides as MAB-Phases. *Inorg. Chem.* **2015**, *54*, 6122–6135. [[CrossRef](#)] [[PubMed](#)]
3. Carlsson, A.; Rosen, J.; Dahlqvist, M. Theoretical predictions of phase stability for orthorhombic and hexagonal ternary MAB phases. *Phys. Chem. Chem. Phys.* **2022**, *24*, 11249–11258. [[CrossRef](#)] [[PubMed](#)]
4. Wang, J.; Ye, T.N.; Gong, Y.; Wu, J.; Miao, N.; Tada, T.; Hosono, H. Discovery of hexagonal ternary phase  $Ti_2InB_2$  and its evolution to layered boride  $TiB$ . *Nat. Commun.* **2019**, *10*, 2284. [[CrossRef](#)]
5. Alameda, L.T.; Moradifar, P.; Metzger, Z.P.; Alem, N.; Schaak, R.E. Topochemical Deintercalation of Al from  $MoAlB$ : Stepwise Etching Pathway, Layered Intergrowth Structures, and Two-Dimensional MBene. *J. Am. Chem. Soc.* **2018**, *140*, 8833–8840. [[CrossRef](#)]
6. Alameda, L.T.; Lord, R.W.; Barr, J.A.; Moradifar, P.; Metzger, Z.P.; Steimle, B.C.; Holder, C.F.; Alem, N.; Sinnott, S.B.; Schaak, R.E. Multi-Step Topochemical Pathway to Metastable  $Mo_2AlB_2$  and Related Two-Dimensional Nanosheet Heterostructures. *J. Am. Chem. Soc.* **2019**, *141*, 10852–10861. [[CrossRef](#)]
7. Zhang, H.; Xiang, H.; zhi Dai, F.; Zhang, Z.; Zhou, Y. First demonstration of possible two-dimensional MBene  $CrB$  derived from MAB phase  $Cr_2AlB_2$ . *J. Mater. Sci. Technol.* **2018**, *34*, 2022–2026. [[CrossRef](#)]
8. Zhang, H.; Dai, F.Z.; Xiang, H.; Wang, X.; Zhang, Z.; Zhou, Y. Phase pure and well crystalline  $Cr_2AlB_2$ : A key precursor for two-dimensional  $CrB$ . *J. Mater. Sci. Technol.* **2019**, *35*, 1593–1600. [[CrossRef](#)]
9. Khazaei, M.; Wang, J.; Estili, M.; Ranjbar, A.; Suehara, S.; Arai, M.; Esfarjani, K.; Yunoki, S. Novel MAB phases and insights into their exfoliation into 2D MBenes. *Nanoscale* **2019**, *11*, 11305–11314. [[CrossRef](#)]
10. Barinov, V.A.; Dorofeev, G.A.; Ovechkin, L.V.; Elskov, E.P.; Ermakov, A.E. Structure and magnetic properties of the  $\alpha$ - $FeB$  phase obtained by mechanical working. *Phys. Status Solidi (a)* **1991**, *123*, 527–534. [[CrossRef](#)]

11. Zhao, X.; Li, L.; Bao, K.; Zhu, P.; Tao, Q.; Ma, S.; Cui, T. Insight the effect of rigid boron chain substructure on mechanical, magnetic and electrical properties of  $\beta$ -FeB. *J. Alloys Compd.* **2022**, *896*, 162767. [[CrossRef](#)]
12. Saldaña, F.I.; Defoy, E.; Janisch, D.; Rouse, G.; Aufran, P.O.; Ghoridi, A.; Séné, A.; Baron, M.; Suescun, L.; Godec, Y.L.; et al. Revealing the Elusive Structure and Reactivity of Iron Boride  $\alpha$ -FeB. *Inorg. Chem.* **2023**, *62*, 2073–2082. [[CrossRef](#)] [[PubMed](#)]
13. Gonzalez Szwacki, N.; Sadrzadeh, A.; Yakobson, B.I. B<sub>80</sub> Fullerene: An Ab Initio Prediction of Geometry, Stability, and Electronic Structure. *Phys. Rev. Lett.* **2007**, *98*, 166804. [[CrossRef](#)] [[PubMed](#)]
14. Szwacki, N.G. Boron Fullerenes: A First-Principles Study. *Nanoscale Res. Lett.* **2007**, *3*, 49. [[CrossRef](#)]
15. Perdew, J.P.; Burke, K.; Ernzerhof, M. Generalized Gradient Approximation Made Simple. *Phys. Rev. Lett.* **1996**, *77*, 3865–3868. [[CrossRef](#)]
16. Blöchl, P.E. Projector augmented-wave method. *Phys. Rev. B* **1994**, *50*, 17953–17979. [[CrossRef](#)]
17. Giannozzi, P.; Baroni, S.; Bonini, N.; Calandra, M.; Car, R.; Cavazzoni, C.; Ceresoli, D.; Chiarotti, G.L.; Cococcioni, M.; Dabo, I.; et al. QUANTUM ESPRESSO: A modular and open-source software project for quantum simulations of materials. *J. Phys. Condens. Matter* **2009**, *21*, 395502. [[CrossRef](#)]
18. Himmetoglu, B.; Janotti, A. Transport properties of KTaO<sub>3</sub> from first-principles. *J. Phys. Condens. Matter* **2016**, *28*, 065502. [[CrossRef](#)]
19. Henkelman, G.; Arnaldsson, A.; Jónsson, H. A fast and robust algorithm for Bader decomposition of charge density. *Comput. Mater. Sci.* **2006**, *36*, 354–360. [[CrossRef](#)]
20. Momma, K.; Izumi, F. VESTA 3 for three-dimensional visualization of crystal, volumetric and morphology data. *J. Appl. Crystallogr.* **2011**, *44*, 1272–1276. [[CrossRef](#)]
21. Bo, T.; Liu, P.F.; Xu, J.; Zhang, J.; Chen, Y.; Eriksson, O.; Wang, F.; Wang, B.T. Hexagonal Ti<sub>2</sub>B<sub>2</sub> monolayer: A promising anode material offering high rate capability for Li-ion and Na-ion batteries. *Phys. Chem. Chem. Phys.* **2018**, *20*, 22168–22178. [[CrossRef](#)] [[PubMed](#)]
22. He, Q.; Li, Z.; Xiao, W.; Zhang, C.; Zhao, Y. Computational investigation of 2D 3d/4d hexagonal transition metal borides for metal-ion batteries. *Electrochim. Acta* **2021**, *384*, 138404. [[CrossRef](#)]
23. Yuan, G.; Bo, T.; Qi, X.; Liu, P.F.; Huang, Z.; Wang, B.T. Monolayer Zr<sub>2</sub>B<sub>2</sub>: A promising two-dimensional anode material for Li-ion batteries. *Appl. Surf. Sci.* **2019**, *480*, 448–453. [[CrossRef](#)]
24. Mir, S.H.; Yadav, V.K.; Singh, J.K. Efficient CO<sub>2</sub> Capture and Activation on Novel Two-Dimensional Transition Metal Borides. *ACS Appl. Mater. Interfaces* **2022**, *14*, 29703–29710. [[CrossRef](#)]
25. Dou, M.; Li, H.; Yao, Q.; Wang, J.; Liu, Y.; Wu, F. Room-temperature ferromagnetism in two-dimensional transition metal borides: A first-principles investigation. *Phys. Chem. Chem. Phys.* **2021**, *23*, 10615–10620. [[CrossRef](#)]
26. Ozdemir, I.; Kadioglu, Y.; Yüksel, Y.; Ümit Akıncı.; Üzengi Aktürk, O.; Aktürk, E.; Ciraci, S. Columnar antiferromagnetic order of a MBene monolayer. *Phys. Rev. B* **2021**, *103*. [[CrossRef](#)]
27. Qi, S.; Fan, Y.; Zhao, L.; Li, W.; Zhao, M. Two-dimensional transition metal borides as highly efficient N<sub>2</sub> fixation catalysts. *Appl. Surf. Sci.* **2021**, *536*, 147742. [[CrossRef](#)]
28. Zhang, B.; Zhou, J.; Guo, Z.; Peng, Q.; Sun, Z. Two-dimensional chromium boride MBenes with high HER catalytic activity. *Appl. Surf. Sci.* **2020**, *500*, 144248. [[CrossRef](#)]
29. Shin, H.; Kang, S.; Koo, J.; Lee, H.; Kim, J.; Kwon, Y. Cohesion energetics of carbon allotropes: Quantum Monte Carlo study. *J. Chem. Phys.* **2014**, *140*, 114702. [[CrossRef](#)]
30. Xu, T.; Wang, Y.; Xiong, Z.; Wang, Y.; Zhou, Y.; Li, X. A Rising 2D Star: Novel MBenes with Excellent Performance in Energy Conversion and storage. *Nano-Micro Lett.* **2022**, *15*, 6. [[CrossRef](#)]
31. Şahin, H.; Cahangirov, S.; Topsakal, M.; Bekaroglu, E.; Akturk, E.; Senger, R.T.; Ciraci, S. Monolayer honeycomb structures of group-IV elements and III-V binary compounds: First-principles calculations. *Phys. Rev. B* **2009**, *80*, 155453. [[CrossRef](#)]
32. Fasolino, A.; Los, J.H.; Katsnelson, M.I. Intrinsic ripples in graphene. *Nat. Mater.* **2007**, *6*, 858–861. [[CrossRef](#)] [[PubMed](#)]
33. Zhang, B.; Zhou, J.; Sun, Z. MBenes: Progress, challenges and future. *J. Mater. Chem. A* **2022**, *10*, 15865–15880. [[CrossRef](#)]
34. Guo, Z.; Zhou, J.; Sun, Z. New two-dimensional transition metal borides for Li ion batteries and electrocatalysis. *J. Mater. Chem. A* **2017**, *5*, 23530–23535. [[CrossRef](#)]

**Disclaimer/Publisher’s Note:** The statements, opinions and data contained in all publications are solely those of the individual author(s) and contributor(s) and not of MDPI and/or the editor(s). MDPI and/or the editor(s) disclaim responsibility for any injury to people or property resulting from any ideas, methods, instructions or products referred to in the content.